

# SCIENTIFIC REPORTS

OPEN

## Switching Correlation and Noise Level in $\text{Pr}^{3+}:\text{YSO}$ Crystal via Dressing Nonlinear Phase

Irfan Ahmed<sup>1,2</sup>, Zhaoyang Zhang<sup>1</sup>, Feng Wen<sup>1</sup>, Da Zhang<sup>1</sup>, Changbiao Li<sup>1</sup>, Ruimin Wang<sup>1</sup> & Yanpeng Zhang<sup>1</sup>

Received: 27 July 2015

Accepted: 24 August 2016

Published: 21 September 2016

We propose and experimentally demonstrate that the intensity noise correlation and the noise level of intensity-difference and intensity-sum in Stokes and anti-Stokes channel can be well controlled by the relative nonlinear phase in spontaneous parametric four-wave mixing process. By modulating the relative nonlinear phase, including self-phase modulation and cross-phase modulation, switching the correlation into anti-correlation and the relative intensity noise level between the intensity-difference and intensity-sum are realized. We also show that the variation tendencies of the relative intensity noise level and the corresponding intensity fluctuations correlation are in accordance with each other.

The experimental preparation, manipulation, and detection of correlated and entangled photon pairs are of great interest for research in fundamental physics and application of quantum information processing<sup>1–3</sup>. Conventionally, entangled photon pairs are produced from spontaneous parametric down-conversion (SPDC) in a nonlinear crystal, where a pump photon is annihilated and two down-converted daughter photons are simultaneously emitted<sup>4</sup>. Entangled photon pairs from spontaneous parametric four-wave mixing in atomic ensemble have also been generated<sup>5</sup>. Compared with the SPDC, the correlated biphotons produced from the SP-FWM have long coherence time (0.1–1.0 s) and narrow spectral width ( $\sim\text{MHz}$ )<sup>6–8</sup>. However, difficulty to integration and miniaturization limits the stepping toward integrated quantum photonic devices via SP-FWM in atomic ensemble. The rare-earth doped crystals, i.e.  $\text{Pr}^{3+}:\text{Y}_2\text{SiO}_3$ , the “atom-like” properties of the dopant can be kept and the atomic coherence can be induced easily when interacting with multiple laser beams, which is different from traditional nonlinear crystal. Recent research progresses related to atomic coherence in such solid-state materials, including electromagnetically induced transparency (EIT)<sup>9</sup>, light velocity reduction and coherent storage<sup>10</sup>, all-optical routing based on optical storage<sup>11</sup>. Besides these, via nonlinear Kerr effects induced by atomic coherence, the correlation switching has been experimentally demonstrated<sup>12</sup>. Such modulation effect is governed by cross-phase modulated (XPM) and self-phase modulated (SPM) in Kerr nonlinear medium<sup>13</sup>.

In this paper, the intensity noise correlation and relative noise level of intensity-difference and intensity-sum in Stokes and anti-Stokes signals are investigated in  $\text{Pr}^{3+}:\text{Y}_2\text{SiO}_3$  crystal. We demonstrated that the switching the correlation into anti-correlation as well as the relative noise about the intensity-difference noise level (IDNL) and intensity-sum noise level (ISNL) can be realized by modulating the relative nonlinear phase, including self-phase modulation and cross-phase modulation. Especially, the correlation and relative noise level can be manipulated by power and polarization of the dressing field participating in the SP-FWM process.

### Results

Figure 1(a) gives the schematic diagram of the experimental arrangement, where the sample (a 3-mm  $\text{Pr}^{3+}:\text{Y}_2\text{SiO}_3$  crystal) is held at 77 K in a cryostat (CFM-102). two tunable dye lasers (with a  $0.04\text{ cm}^{-1}$  linewidth) pumped by an injection locked single-mode Nd:YAG laser (Continuum Powerlite DLS 9010, 10 Hz repetition rate, 5 ns pulse width) are used to generate the pumping fields  $E_1$  ( $\omega_1, \Delta_1$ ) and  $E_2$  ( $\omega_2, \Delta_2$ ) with the frequency detuning of  $\Delta_i = \omega_{mn} - \omega_i$  ( $i = 1, 2$ ), respectively, where  $\Omega_{mn}$  is the transition frequency between level  $|m\rangle$  and  $|n\rangle$ .  $E_1$  drives the transition  $|0\rangle \rightarrow |1\rangle$ , and  $E_2$  couples to the transition  $|0\rangle \rightarrow |2\rangle$ . Specifically, the horizontally polarized pumping beam  $E_1$  with peak power of about 6 kW and beam waist of  $280\ \mu\text{m}$  is combined with pumping beam  $E_2$  (about 12 kW) at an angle of 3 mrad at the center of  $\text{Pr}^{3+}:\text{Y}_2\text{SiO}_3$  crystal, where  $E_1$  crosses with  $E_2$  and amplified with a

<sup>1</sup>Key Laboratory for Physical Electronics and Devices of the Ministry of Education & School of Science & Shaanxi Key Lab of Information Photonic Technique, Xi'an Jiaotong University, Xi'an 710049, China. <sup>2</sup>Department of Electrical Engineering, Sukkur IBA, Sukkur 65200, Pakistan. Correspondence and requests for materials should be addressed to R.W. (email: wangrm@mail.xjtu.edu.cn) or Y.Z. (email: ypzhang@mail.xjtu.edu.cn)

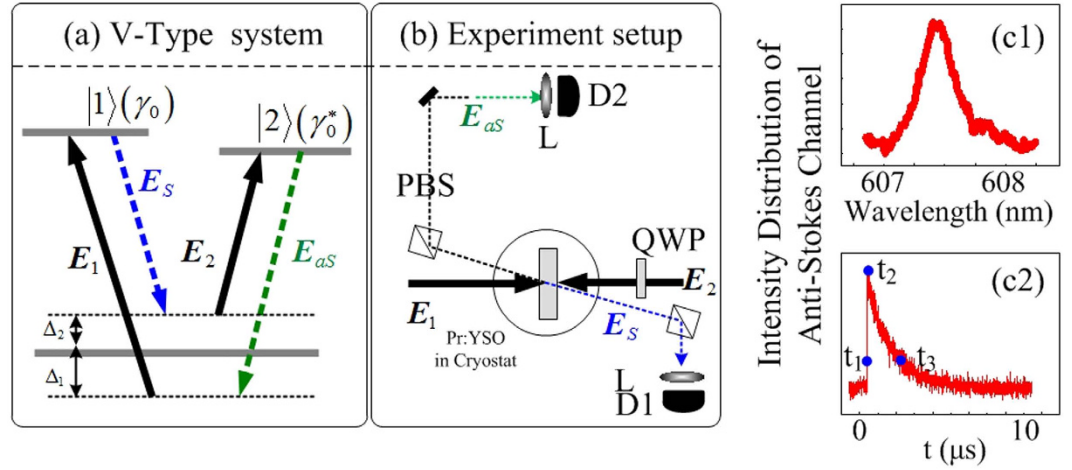


**Figure 1.** (a) Three-level system (V-type) in Pr<sup>3+</sup>:YSO crystal and the laser coupling configuration. (b) Experimental setup scheme. D: photomultiplier tube, PBS: polarized beam splitter, BS: beam splitter, and L: lens, QWP: quarter wave plate. (c1,c2) shows intensity distribution of anti-Stokes in frequency and time domain, respectively.

gain of  $G \approx 3.5$ . Based on these settings, two narrow band correlated photons pairs (Stokes  $E_S$  and anti-Stokes  $E_{AS}$ ) are generated via SP-FWM process, and the corresponding photon counting rate for Stokes and anti-Stokes channel are  $1 \times 10^6 \text{ s}^{-1}$  and  $6 \times 10^7 \text{ s}^{-1}$ , respectively.

When two pumping field  $E_1$  and  $E_2$  are switched on, in the V-type three-level  $|1\rangle \rightarrow |0\rangle \rightarrow |2\rangle$ , two narrow band correlated photons (Stokes field  $E_S$  and anti-Stokes field  $E_{AS}$ ) are generated via SP-FWM process, satisfying the phase-matching condition  $\mathbf{k}_1 + \mathbf{k}_2 = \mathbf{k}_{AS} + \mathbf{k}_S$ . Figure 1(b) shows the experimental arrangement taking into account the above phase-matching conditions. The generated Stokes signal  $E_S$  and anti-Stokes signal  $E_{AS}$  are reflected by polarized beam splitters (PBS) and detected by photomultiplier tubes, and recorded by D<sub>1</sub> and D<sub>2</sub>. To study fluctuations in Stokes and anti-Stokes channel transmitted through Pr<sup>3+</sup>:YSO, the dependence of the intensities on time and frequency are registered by digital oscilloscope and photomultiplier tubes, respectively, as shown in Fig. 1(c1,c2), and then the obtained noises in Stokes and anti-Stokes channel are analyzed by two methods. On one hand, by using intensity fluctuations  $\delta I_i(t)$  ( $i = AS, S$ ) recorded by digital oscilloscope, the temporal waveform correlations between Stokes and anti-Stokes channel are investigated by Eq. (6) under a variety of conditions. On the other hand, by using intensity fluctuations recorded by photomultiplier tubes, the measured intensity fluctuations in Stokes and anti-Stokes channel are subtracted and added from each other, and are then analyzed with a spectrum analyzer to investigate the relative noise power between intensity-difference and intensity-sum, as indicated by Eq. (7). Here, Fig. 1(c1,c2) show the measured intensity of anti-Stokes signal in frequency and time domain, respectively.

In the interaction picture, the coupled Stokes channel and anti-Stokes channel can be described by

$$H = \kappa(a_{AS}^+ a_S^+ + a_{AS} a_S) \tag{1}$$

where  $\kappa = |\chi^{(3)} \mathbf{E}_1 \mathbf{E}_1| = |N \mu_{10}^2 \rho_{S/AS}^{(3)} / \hbar \epsilon_0 G_{S/AS}|$  and  $\kappa$  is called the coupling parameter of the SP-FWM, depending on the nonlinearity coefficient  $\chi^{(3)}$  and intensity of the pump field, and  $a_{AS}^+$  ( $a_S^+$ ) is boson annihilation operator acting on  $E_{AS}$  ( $E_S$ ) channel,  $G_{Si} = \mu_i \mathbf{E}_i / \hbar$  Rabi frequency of  $\mathbf{E}_{Si}$  ( $i = 1, 2, 3$ ),  $\mu_{ij}$  electric dipole moment between energy state  $|i\rangle$  and  $|j\rangle$ , and  $N$  averaged atomic density. According to the Liouville pathways [8], via the dressed perturbation chains of  $\rho_{00}^{(0)} \xrightarrow{\omega_1} \rho_{10}^{(1)} \xrightarrow{\omega_s} \rho_{00}^{(2)} \xrightarrow{\omega_2} \rho_{AS}^{(3)} (E_{AS})$  and  $\rho_{00}^{(0)} \xrightarrow{\omega_2} \rho_{02}^{(1)} \xrightarrow{\omega_{AS}} \rho_{00}^{(2)} \xrightarrow{\omega_1} \rho_S^{(3)} (E_S)$ , the density-matrix element for  $E_S$  and  $E_{AS}$  can be expressed as  $\rho_S^{(3)} = -iG_{AS}^* G_1 G_2 / (d_{20} d_{10} d_{00})$  and  $\rho_{AS}^{(3)} = -iG_S^* G_1 G_2 / (d_{10} d_{20} d'_{00})$ , where  $G_i = \mu_i E_i / \hbar$  ( $i = 1, 2$ ) is the Rabi frequency of the field  $E_i$ , and  $\Gamma_{ij}$  is the decay rate between the energy levels  $|i\rangle$  and  $|j\rangle$ .  $d_{20} = \Gamma_{20} + i\Delta_2$ ,  $d_{10} = \Gamma_{10} + i\Delta_1$ ,  $d_{00} = \Gamma_{00} + i(\Delta_2 - \Delta_1)$ ,  $d'_{00} = \Gamma_{00} + i(\Delta_1 - \Delta_2)$ .

Next, taking the dressing effects of  $E_1$  and  $E_2$  into account, the revised density-matrix element for  $E_S$  and  $E_{AS}$  can be rewritten as

$$\rho_S^{(3)} = \frac{-iG_{AS}^* G_1 G_2}{d_{20}(d_{00} + |G_2|^2 / [d'_{20} + |G_2|^2 / d_{01}]) (d_{10} + |G_1|^2 / \Gamma_{11})} \tag{2}$$

$$\rho_{AS}^{(3)} = \frac{-iG_S^* G_1 G_2}{d_{10}(d'_{00} + |G_2|^2 / [\Gamma_{20} + |G_1|^2 / d_{21}]) (d_{20} + |G_1|^2 / \Gamma_{22})} \tag{3}$$

where  $d'_{20} = \Gamma_{20} + i(\Delta_2 - \Delta_1)$ ,  $d_{21} = \Gamma_{21} - i\Delta_1$ ,  $d_{01} = \Gamma_{01} - i\Delta_1$ .

In addition, the polarization of  $E_2$  is modulated by inserting a quarter-wave plate (QW) in  $E_2$  beam (see Fig. 1(b)), while pumping field  $E_1$  is kept linearly polarized. The vertically polarized components (S-polarization)

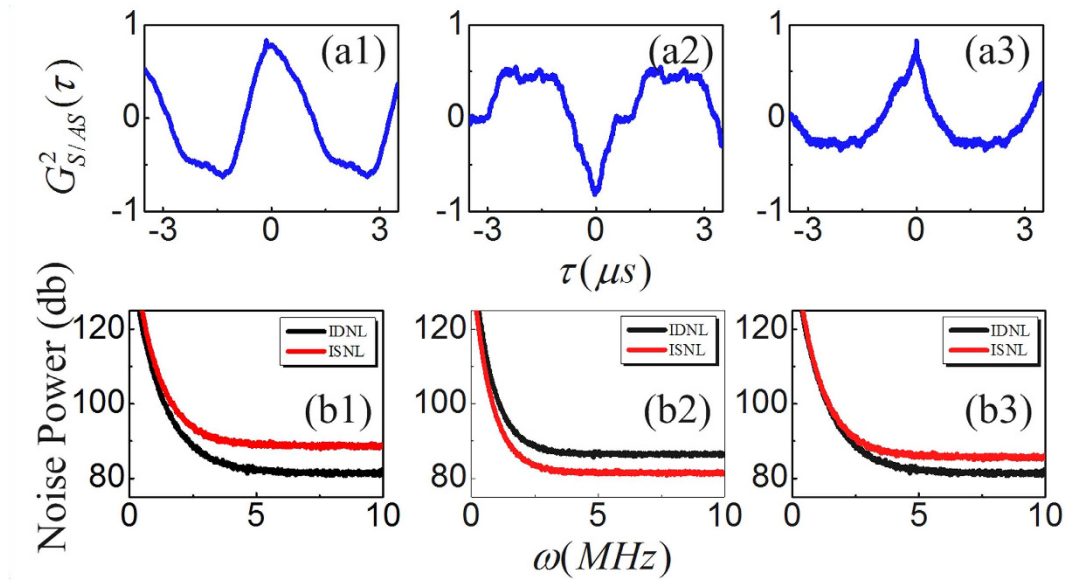


**Figure 2.** The noise correlations and the relative intensity noise level between IDNL and ISNL of  $E_{AS}$  and  $E_S$  are shown in (a1–a3,b1–b3), respectively, with  $P_1 = 4\text{mW}$ , and  $P_2 = 6, 8, \text{ and } 10\text{mW}$ .

of Stokes and anti-Stokes signals reflected by PBS are detected. Therefore, the effective density matrix elements for  $E_S$  and  $E_{AS}$  are given by

$$\rho_{S(y)}^{(3)} = \rho_{S(xyxy)}^{(3)} + \rho_{S(yyyy)}^{(3)} \quad (4)$$

$$\rho_{AS(y)}^{(3)} = \rho_{AS(xyxy)}^{(3)} + \rho_{AS(yyyy)}^{(3)} \quad (5)$$

In this case, the Rabi frequency  $|G_2|^2$  in Eq. (2) is replaced by  $C_x^2(\cos^4 \theta + \sin^4 \theta)|G_2|^2$  for matrix element  $\rho_{(xyxy)}^{(3)}$  and  $C_y^2(2 \cos^2 \theta \sin^2 \theta)|G_2|^2$  for  $\rho_{(yyyy)}^{(3)}$ , respectively. Where  $c_{x,y}$  is the anisotropic factor in different directions of crystal,  $\theta$  is the rotated angle of the QWP's axis from the  $x$  axis.

Based on the measurements of the second-order coherence functions, See Methods for theoretical derivations of the intensity distribution at each output channel, the intensity fluctuations correlation between the Stokes and anti-Stokes signals<sup>14–16</sup> can be obtained as

$$G_{S-as}^{(2)}(\tau_1) = \frac{\langle (\delta \hat{I}_S(t_S)) (\delta \hat{I}_{as}(t_{as})) \rangle |\Theta(\tau)|^2}{\sqrt{\langle (\delta \hat{I}_S(t_S))^2 \rangle \langle (\delta \hat{I}_{as}(t_{as}))^2 \rangle}} = \frac{C_{S-as} |\Theta(\tau)|^2}{\sqrt{|C_S|^2 |C_{as}|^2}} \cos(\Delta\varphi) \quad (6)$$

where averaging over the time is defined as  $\langle I(t) \rangle = \frac{1}{T} \int_t^{t+T} I(t) dt$ ,  $\tau = t_S - t_{AS}$  is the selected time delay between Stokes and anti-Stokes signal, and  $T$  is the time of integration, in our case  $T = 10 \mu\text{s}$ .  $\Delta\varphi = \varphi_S - \varphi_{AS}$  is relative nonlinear phase between Stokes and anti-Stokes signal based on XPM and SPM.

Different from the intensity-difference squeezing<sup>15</sup>, we investigate the relative noise power between the intensity-difference and intensity-sum in V-type systems, which can be modified as<sup>17–19</sup>

$$Sq = \text{Log}_{10} \left[ \frac{\langle \delta^2(\hat{I}_S - \hat{I}_{AS}) \rangle}{\langle \delta^2(\hat{I}_S + \hat{I}_{AS}) \rangle} \right] \cos(\Delta\varphi) |\Theta(\tau)|^2 \quad (7)$$

where  $\langle \delta^2(\hat{I}_S - \hat{I}_{AS}) \rangle$  and  $\langle \delta^2(\hat{I}_S + \hat{I}_{AS}) \rangle$  are mean square deviation of intensity fluctuations difference and sums between Stokes and anti-Stokes signal, respectively,  $\Theta(\tau)$  is two photon envelop function.

To study the role of the relative nonlinear phase played on intensity fluctuations correlation as well as the intensity noise level between the IDNL and ISNL of anti-Stokes and Stokes beams, the dependence of the intensities on time  $\langle I_i \rangle + \delta I_i(t)$  ( $i = AS, S$ ) are registered. Here  $\langle I_i \rangle$  is the average intensity of anti-Stokes/Stokes beams, and  $\delta I_i(t)$  are corresponding intensity fluctuations. After the intensity fluctuations is averaged by a fast gated integrator over 10 pulses, and then using the averaged data, the correlation curve is calculated via cross correlation of the intensity fluctuation in stokes and anti-stokes channel.

Figure 2(a) shows the fluctuation correlations between  $E_{AS}$  and  $E_S$  under different dressing powers, where the curve is calculated by substituting the recorded intensity fluctuations  $\delta I_{AS,S}(t)$  into Eq. (6) setting  $\Delta_1 = \Delta_2 = 0$  and  $P_1 = 4\text{mW}$ . When  $P_2 = 6\text{mW}$ , as shown in Fig. 2(a1), the correlation peak  $G_{S/AS}^{(2)}(\tau)$  at delay time  $\tau = 0$  has amplitude of  $0.83 \pm 0.01$  and corresponding full width at half maximum (FWHM) is  $2.2 \mu\text{s}$ . If we set the power of  $E_2$  at  $P_2 = 8\text{mW}$ , as shown in Fig. 2(a2), we find the amplitude of correlation peak  $G_{S/AS}^{(2)}(\tau)$  at  $\tau = 0$  is switched from

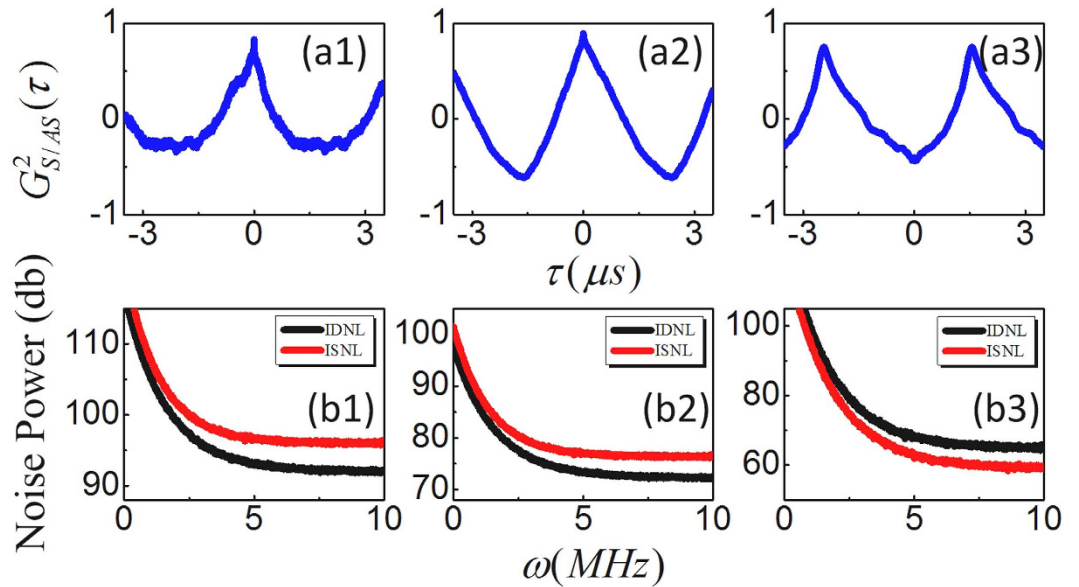


**Figure 3.** Same as Fig. 2 but with changing polarization of  $E_2$  from linear (a1,b1), elliptical (a2,b2), and to circular (a3,b3).

positive ( $0.83 \pm 0.01$ ) to negative ( $-0.82 \pm 0.01$ ), therefore, the intensity fluctuations is changed from correlated to anti-correlated. The FWHM of the correlation peaks has increased to  $1.8 \mu\text{s}$ . In contrast, at  $P_2 = 10 \text{ mW}$ , the correlation peak  $G_{S/AS}^{(2)}(\tau)$  at  $\tau = 0$  is adjusted back to correlated with amplitude  $0.83 \pm 0.01$  and corresponding FWHM is further increased to  $1.5 \mu\text{s}$ , as shown in Fig. 2(a3). These results may be explained by nonlinear refractive index of Kerr medium. Since the dressing state (created by  $E_2$ ) can modulate the nonlinear refractive index of Kerr medium and lead to XPM, the relative nonlinear phase between Stokes and anti-Stokes signal  $\Delta\varphi = 2(k_S n_2^S - k_{AS} n_2^{AS})|E_2|^2 e^{-r^2} z/n_1$  can be significantly modulated. Where  $\Delta\varphi = \varphi_S - \varphi_{AS}$  is the relative nonlinear phase between Stokes and anti-Stokes signal based on XPM, whereas  $\varphi_S$  ( $\varphi_{AS}$ ) is nonlinear phases induced on Stokes (anti-Stokes) signal, respectively and  $r$  is the beam radius of Gaussian beam incident from laser and  $z$  is length of YSO crystal's lens ( $z = 3 \text{ mm}$ ). Specifically, by changing the power of  $E_2$  at 6, 8, and 10 mW, the relative nonlinear phase between Stokes and anti-Stokes are modulated to  $\Delta\varphi = 0, \pi$ , and  $2\pi$ , respectively. Therefore,  $G_{S/AS}^{(2)}(\tau)$  at  $P_2 = 6 \text{ mW}$  and  $10 \text{ mW}$  have positive correlation peak, and at  $P_2 = 8 \text{ mW}$  have negative correlation peak.

On the other hand, by substituting  $\delta I_{AS,S}(t)$  into Eq. (7), the influence of the nonlinear phase on the relative intensity noise level between the intensity-difference and intensity-sum are also investigated. To measure the relative noise level between the IDNL and ISNL, we use two balance detector to pick up the noise in stokes and anti-stokes channel, where the two coherent beams (not shown in Fig. 1), one have the same intensity with stokes and another have same intensity with anti-stokes, are used to illuminate to two detectors during measurement. The measured noise in stokes and anti-stokes are subtracted and added from each other, and then analyzed with a spectrum analyzer. Figure 2(b1–b3) demonstrated that noise level of the intensity-difference signal (IDNL, black curve) can be switched higher or lower than the intensity-sum signal (ISNL, red curve) by changing  $\Delta\varphi = 0, \pi$ , and  $2\pi$ , respectively. we can see that the noise level of intensity-difference signal is lower than the intensity-sum signal when  $\Delta\varphi = 0$  and  $2\pi$ , as in Fig. 2(b1,b3), while the relative noise level of intensity-difference is switched higher than intensity-sum when  $\Delta\varphi = \pi$ , see Fig. 2(b2). It is worth mentioning that the variation tendencies of the intensity noise level between the intensity-difference and intensity-sum and the corresponding intensity fluctuations correlation are in accordance with each other. Therefore, intensity fluctuations correlation and relative intensity noise level depends crucially on the relative nonlinear phase induced by XPM.

The modulation of the nonlinear phase can be realized not only by changing the power of  $E_2$ , but changing the polarization of  $E_2$  as well. As stated above, the polarization of the dressing field  $E_2$  can be controlled by inserting a QWP, and the effective Rabi frequency of  $E_2$  for matrix element  $\rho_{(xxyy)}^{(3)}$  is  $C_x^2 (\cos^4 \theta + \sin^4 \theta) |G_2|^2$ , and for  $\rho_{(yyyy)}^{(3)}$  is  $C_y^2 (2 \cos^2 \theta \sin^2 \theta) |G_2|^2$ . Based on above discussion, the matrix element  $\rho_{(xxyy)}^{(3)}$  ( $\rho_{(yyyy)}^{(3)}$ ) and corresponding third-order effective susceptibility can be modulated by the rotating the angle of QWP therefore, the nonlinear phase to detected signal can also be modulated.

Now, we focus on the polarization dependences of the intensity fluctuations correlation and the relative intensity noise level between IDNL and ISNL. Modulated polarization can be achieved by inserting QWP in Fig. 1(b) in front of incident beam  $E_2$ . Figure 3(a1–a3) show the correlation curves at linear polarization ( $\theta = 0$ ), elliptical polarization ( $\theta = \pi/6$ ), and circular polarization ( $\theta = \pi/4$ ), respectively, with setting  $\Delta_1 = \Delta_2 = 0$ ,  $P_1 = 5 \text{ mW}$  and  $P_2 = 10 \text{ mW}$ . We can see from Fig. 3(a1–a3) that intensity fluctuations is changed from correlated to anti-correlated as polarization modulated from linear to circular polarization. In addition, the relative intensity noise level between the IDNL and ISNL of the output beams  $E_{AS}$  and  $E_S$  depends crucially on the correlation functions, therefore, the corresponding relative noise level of intensity-difference is switched from

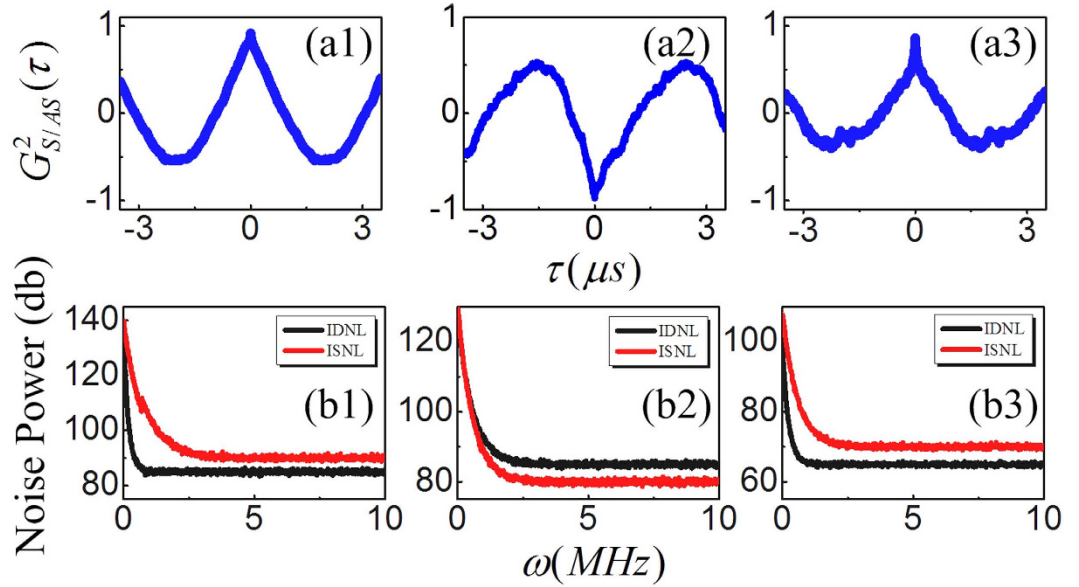


**Figure 4.** By selecting  $t_1$ ,  $t_2$ , and  $t_3$  in decay curves as shown in Fig. 1(c2), the noise correlations and the relative intensity noise between IDNL and ISNL are demonstrated in (a1–a3,b1–b3), respectively.

lower than the intensity-sum to higher than the intensity-sum as polarization modulated from linear to circular. This phenomenon can be interpreted from Eqs (2)–(5), where relative nonlinear phase  $\Delta\varphi = 2(k_S n_{2a}^S - k_{AS} n_{2a}^{AS}) |E_2|^2 \cos \theta (e^{-r^2} z) / n_1$  ( $a = 0, +, \text{ and } -$  are corresponding to linear, left circular, and right circular polarization, respectively.) induced by XPM at circular polarization is about  $\pi$ , and at linear ( $\theta = 0$ ) and elliptical ( $\theta = \pi/6$ ) polarization is about 0 and  $2\pi$ . Therefore, relative intensity noise level between IDNL and ISNL and correlation can also be switched by polarization of pumping field.

## Discussion

Finally, by selecting different timing position in decay curves, see Fig. 1(c2), the noise correlations and relative intensity noise level between the IDNL and ISNL of the output beams  $E_{AS}$  and  $E_S$  are demonstrated, as shown in Fig. 4(a,b), respectively, where those curves are calculated under fixing  $\Delta_1 = \Delta_2 = 0$  and setting  $P_1 = 5$  mW and  $P_2 = 10$  mW. At the high intensity time position (2<sup>nd</sup>),  $G_{S/AS}^{(2)}(\tau)$  is obtained as shown in Fig. 4(a2), where the correlation peak at  $\tau = 0$  has amplitude  $-0.88 \pm 0.01$  and corresponding FWHM is  $1.6 \mu\text{s}$ . It is interesting that the correlation is switched to correlation with amplitude  $0.86 \pm 0.01$  and  $0.89 \pm 0.01$  at the lower intensity time position (1<sup>st</sup>) and (3<sup>rd</sup>), respectively. This phenomenon are tightly related to the intensity of generated field  $E_{AS}$  and  $E_S$ , and can be explained by relative nonlinear phase induced by SPM  $\Delta\varphi_1 = 2(|E_S|^2 n_2^S - |E_{AS}|^2 n_2^{AS}) \zeta e^{-r^2} z / n_1$ , here  $\zeta = |G_2 / G_{S/AS}|^2$  is intensity ratio of strong field  $G_2$  and obtained weak fields  $G_{S/AS}$ . The SPM is significantly at 2<sup>nd</sup> for intensity of  $E_{AS}$  and  $E_S$  are the largest at this timing point, therefore, the relative phase induced by SPM at 2<sup>nd</sup> is about  $\Delta\varphi \cong \pi$ . On the other hand, at 1<sup>st</sup> and 3<sup>rd</sup>, the SPM can be ignored for faint intensity of  $E_{AS}$  and  $E_S$ , therefore, the relative phase between Stokes and anti-Stokes is same  $\Delta\varphi \cong 0$ , which is the reason that Fig. 4(a1,a3) are almost symmetrical to each other. With the same reason, the IDNL is demonstrating significantly higher than intensity-sum signal at 2<sup>nd</sup> (Fig. 4(b3)), and lower than ISNL at 1<sup>st</sup> and 3<sup>rd</sup>. Therefore, intensity fluctuations correlation and the relative intensity noise level between IDNL and ISNL also depend crucially on the relative nonlinear phase induced by SPM.

The dressed noise correlation and the relative intensity noise level between IDNL and ISNL based on SP-FWM process in  $\text{Pr}^{3+}:\text{Y}_2\text{SiO}_3$  crystals have been observed experimentally and explained theoretically. We observed that the correlation and the relative intensity noise level between IDNL and ISNL can be switched by controlling the power and polarization of the dressing field. These results are attributed to dressing-induced self-phase modulation and cross-phase modulation. The investigation may find applications in all-solids quantum communication and quantum information processing.

## Methods

**Experimental setup.** The sample used in present experiments is a 0.05% rare-earth  $\text{Pr}^{3+}$  doped  $\text{Y}_2\text{SiO}_3$  ( $\text{Pr}^{3+}:\text{Y}_2\text{SiO}_3$ ) crystal, and the triplet energy-level ( $^3H_4$ ) and singlet energy-level ( $^1D_2$ ) of  $\text{Pr}^{3+}$  are selected which can be distinguished by investigating the optical spectrum of  $\text{Pr}^{3+}$ . The degeneracy of the energy levels of the  $\text{Pr}^{3+}$  ion is removed by the crystal field of YSO, where the terms in  $^3H_4$  and  $^1D_2$  states are split into nine and five Stark components, respectively. The  $\text{Pr}^{3+}$  impurity ions occupy two nonequivalent cation sites (sites I and II, respectively) in the YSO crystal lattice. The energy levels are labeled by a Greek letters with and without asterisk for site II and I sites, respectively. The coupling between  $\text{Pr}^{3+}$  ions localized at different cation vacancies can happen due to induced dipole-dipole interactions, so one can treat the two ions as a hetero-nuclear-like molecule. Therefore,

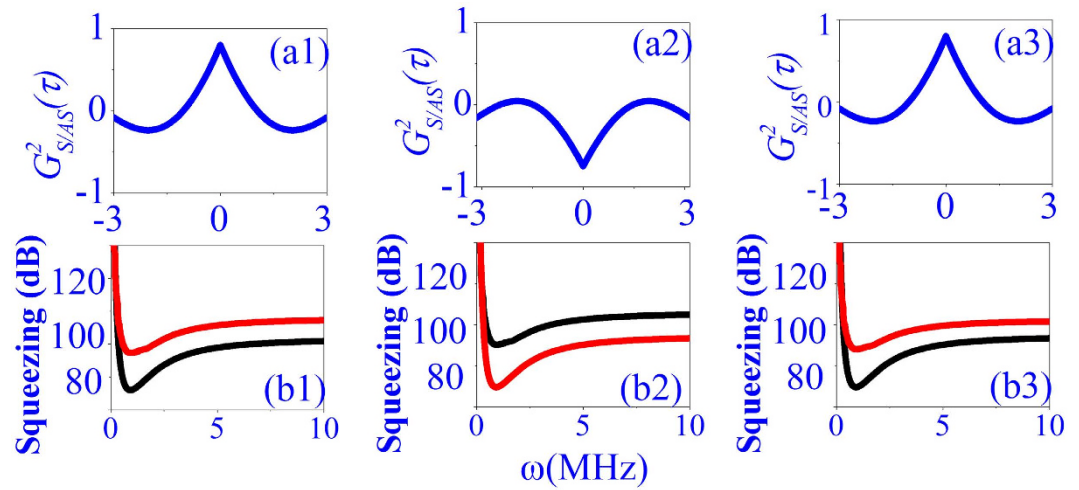


**Figure 5.** The simulated plots of noise correlations and the relative intensity noise level between IDNL and ISNL of  $E_{AS}$  and  $E_S$  are shown in (a1–a3,b1–b3), respectively in accordance with experimental conditions defined in Fig. 2.

we can construct a V-type three-level subsystem  $|0\rangle(\delta_0) \rightarrow |1\rangle(\gamma_0) \rightarrow |2\rangle(\gamma_0^*)$  by coupling the corresponding laser fields as shown in Fig. 1(a).

**Theoretical models for the intensity distribution in each output channel.** When the generated Stokes and anti-Stokes signals passes through the  $\text{Pr}^{3+}:\text{Y}_2\text{SiO}_3$  crystal along the  $z$  axis, the nonlinear cross-phase modulation as well as self-phase modulation is acquired. According to Eq. (1), the propagation dynamics for  $a_{AS}^+$  and  $a_S^+$  at the output surface of is determined by<sup>20–22</sup>,

$$da_S/dt = \gamma_S a_S + \chi_S^{(3)} a_{AS}^+ \exp(i\varphi_S) \quad (8)$$

$$da_{AS}/dt = \gamma_{AS} a_{AS} + \chi_{AS}^{(3)} a_S^+ \exp(i\varphi_{AS}) \quad (9)$$

where nonlinear susceptibility coefficients  $\chi_i^{(3)}$  is proportional to  $\mu N \rho_i^{(3)}/(\epsilon_0 E_1 E_2 E_i^*)$ .  $\varphi_S$  ( $\varphi_{AS}$ ) is nonlinear phases induced on Stokes (anti-Stokes) signal, respectively, and the relative nonlinear phase between Stokes and anti-Stokes signal can be defined as  $\Delta\varphi = \varphi_S - \varphi_{AS}$ . Here, the induced nonlinear phase shift  $\Delta\varphi$  can be defined as  $\varphi_i = 2(k_i n_2^i |E_1|^2 e^{-r^2 z})/n_1$ , where  $n_2^i = \text{Re} \chi_i^{(3)}/\epsilon_0 c n_1$  is self or cross-Kerr nonlinear coefficient for Stokes (anti-Stokes) field, and  $n_1$  is the linear refractive index. Therefore, from Eqs (4) and (5), the photon number from output of Stokes/anti-Stokes channel can be solved as

$$\begin{aligned} \hat{N}_S &= \hat{a}_S^+(L)\hat{a}_S(L) = G\hat{a}_S^+(0)\hat{a}_S(0) + (G-1)\hat{a}_{AS}(0)\hat{a}_{AS}^+(0) \\ &+ \sqrt{G(G-1)}\hat{a}_S^+(0)\hat{a}_{AS}^+(0) + \sqrt{G(G-1)}\hat{a}_{AS}(0)\hat{a}_S(0) \end{aligned} \quad (10)$$

$$\begin{aligned} \hat{N}_{AS} &= \hat{a}_{AS}^+(L)\hat{a}_{AS}(L) = G\hat{a}_{AS}^+(0)\hat{a}_{AS}(0) + (G-1)\hat{a}_S(0)\hat{a}_S^+(0) \\ &+ \sqrt{F(G-1)}\hat{a}_{AS}^+(0)\hat{a}_S^+(0) + \sqrt{G(G-1)}\hat{a}_S(0)\hat{a}_{AS}(0) \end{aligned} \quad (11)$$

where the gain coefficient  $G = \cosh(2\chi_i^{(3)}L)$  is deduced as function of nonlinear susceptibility, and the intensity at each output channel proportional to the measured photon number can be written as  $I_i(t_i) = N_i e^{-\Gamma_i t_i}$ .

According to the Liouville pathways  $\rho_{00}^{(0)} \xrightarrow{\omega_1} \rho_{10}^{(1)} \xrightarrow{\omega_2} \rho_{00}^{(2)} \xrightarrow{\omega_3} \rho_{AS}^{(3)}(E_{AS})$  and  $\rho_{00}^{(0)} \xrightarrow{\omega_2} \rho_{02}^{(1)} \xrightarrow{\omega_{AS}} \rho_{00}^{(2)} \xrightarrow{\omega_1} \rho_S^{(3)}(E_S)$ , the non-steady state solutions of density-matrix element for  $E_S$  and  $E_{AS}$  can be expressed as

$$\begin{aligned} \rho_S^{(3)} &= \left(\frac{i\mu_1}{\hbar}\right)\left(\frac{i\mu_2}{\hbar}\right)\left(\frac{i\mu_{AS}}{\hbar}\right) e^{i\omega_S} \int_0^\infty dt_3 \int_0^\infty dt_{AS} \int_0^\infty dt_1 A_1(r, t - t_1 - t_{AS} - t_3) \\ &\times [A_S(r, t - t_{AS} - t_3)]^* A_3(r, t - t_3) e^{-(\Gamma_{10} + i\Delta_1)t_1} e^{-(\Gamma_{00} + i(\Delta_2 - \Delta_1))t_{AS}} e^{-(\Gamma_{20} + i\Delta_2)t_3} \end{aligned} \quad (12)$$

$$\begin{aligned} \rho_{AS}^{(3)} &= \left(\frac{i\mu_1}{\hbar}\right)\left(\frac{i\mu_2}{\hbar}\right)\left(\frac{i\mu_S}{\hbar}\right) e^{i\omega_{AS}} \int_0^\infty dt_3 \int_0^\infty dt_S \int_0^\infty dt_1 A_1(r, t - t_1 - t_S - t_3) \\ &\times [A_S(r, t - t_S - t_3)]^* A_3(r, t - t_3) e^{-(\Gamma_{10} + i\Delta_1)t_1} e^{-(\Gamma_{00} + i(\Delta_1 - \Delta_2))t_S} e^{-(\Gamma_{20} + i\Delta_2)t_3} \end{aligned} \quad (13)$$

where  $A_i(r, t) = E_i e^{ik_r r}$ .

In addition, taking the population distributions in levels  $|1\rangle$  and  $|2\rangle$  into account, where the Boltzmann distribution with finite temperature is considered in the deduction, the two-photon envelope function  $\Theta(\tau)$  is obtained as

$$\Theta(\tau) = C_0 \int e^{-i(\varpi_s \tau_s + \varpi_{as} \tau_{as})} \rho_n^{(3)}(\delta) e^{i\delta\tau} d\delta = C_0 C_1 e^{-i(\varpi_s \tau_s + \varpi_{as} \tau_{as})} [e^{i\delta_+ \tau} e^{-\Gamma_+ \tau} - e^{i\delta_- \tau} e^{-\Gamma_- \tau}] \quad (14)$$

where  $C_0$  and  $C_1$  are time independent constants, and  $n = AS/S$  and  $\delta_{\pm} = \Delta_1 \pm \sqrt{G_1^2 + \Delta_1^2 + 4\Gamma_{10}\Gamma_{30}}/2$ . The first term in the square brackets on the right-hand side of Eq. (14) represents the two-photon amplitude between correlated photons peaking at  $\varpi_s = \omega_1 - \delta_+$  and  $\varpi_{AS} = \omega_1 + \delta_+$  with linewidth  $\Gamma_+$ , while the second term stands for the two-photon amplitude between paired photons centered at  $\varpi_s = \omega_1 - \delta_-$  and  $\varpi_{AS} = \omega_1 + \delta_-$  with linewidth  $\Gamma_-$ . The sum of these two amplitudes is manifested by a slowly oscillating phase term.

Finally, the simulated plots of noise correlations and the relative intensity noise level between IDNL and ISNL of  $E_{AS}$  and  $E_S$  are shown in Fig. 5(a1–a3, b1–b3), respectively in accordance with experimental conditions defined in Fig. 2 and have been calculated using Eq. (6) involving relative non linear phase. Figure 5(a1–a3), shows simulation plots of second order correlation function  $G_{S/AS}^{(2)}(\tau)$  at delay time  $\tau = 0$ . The results of correlation in Fig. 2(a1–a3) precisely match the simulated plots involving the phase shift in Fig. 5(a1–a3). Besides, Fig. 5(a1–a3) shown the theoretical plots for relative intensity noise level between IDNL and ISNL. The simulated plots of IDNL and ISNL precisely matches with obtained experimental plots of IDNL and ISNL and are calculated using Eq. (7).

## References

- Gisin, N., Ribordy, G., Tittel, W. & Zbinden, H. Quantum cryptography. *Reviews of Modern Physics*, **74**, 145–195 (2002).
- Yamamoto, Y. & Haus, H. A. Preparation, measurement and information capacity of optical quantum states. *Reviews of Modern Physics*, **58**, 1001–1020 (1986).
- Horodecki, R., Horodecki, P., Horodecki, M. & Horodecki, K. Quantum entanglement. *Reviews of Modern Physics*, **81**, 865–942 (2009).
- Rubin, M. H., Klyshko, D. N., Shih, Y. H. & Sergienko, A. V. Theory of two-photon entanglement in type-II optical parametric down-conversion. *Phys. Rev. A* **50**, 5122–5133 (1994).
- Balić, V., Braje, D. A., Kolchin, P., Yin, G. Y. & Harris, S. E. Generation of Paired Photons with Controllable Waveforms. *Phys. Rev. Lett.* **94**, 183601 (2005).
- Thompson, J. K., Simon, J., Loh, H. & Vuletić, V. A High-Brightness Source of Narrowband, Identical-Photon Pairs. *Science*, **313**, 74–77 (2006).
- Du, S., Wen, J., Rubin, M. H. & Yin, G. Y. Four-Wave Mixing and Biphoton Generation in a Two-Level System. *Phys. Rev. Lett.* **98**, 053601 (2007).
- Wen, F. *et al.* Multidressed suppression and enhancement of spontaneous parametric four-wave-mixing processes. *J. Opt. Soc. Am. B*, **31**, 2384–2389 (2014).
- Phillips, M. C. *et al.* Electromagnetically Induced Transparency in Semiconductors via Biexciton Coherence. *Phys. Rev. Lett.* **91**, 183602 (2003).
- Heinze, G., Hubrich, C. & Halfmann, T. Stopped Light and Image Storage by Electromagnetically Induced Transparency up to the Regime of One Minute. *Phys. Rev. Lett.* **111**, 033601 (2013).
- Wang, H. H. *et al.* All-optical routing by light storage in a  $\text{Pr}^{3+}:\text{Y}_2\text{SiO}_5$  crystal. *Applied Physics Letters*, **93**, 221112–221113 (2008).
- Wei, C. & Manson, N. B. Observation of electromagnetically induced transparency within an electron spin resonance transition. *Journal of Optics B Quantum & Semi classical Optics*, **1**, 464–468 (1999).
- Yan, M., Rickey, E. G. & Zhu, Y. Observation of doubly dressed states in cold atoms. *Phys. Rev. A* **64**, 013412 (2001).
- Wu, H. & Xiao, M. Bright correlated twin beams from an atomic ensemble in the optical cavity. *Phys. Rev. A* **80**, 063415 (2009).
- Qin, Z. Z. *et al.* Experimental Generation of Multiple Quantum Correlated Beams from Hot Rubidium Vapor. *Phys. Rev. Lett.* **113**, 023602 (2014).
- Sautenkov, V. A., Rostovtsev, Y. V. & Scully, M. O. Switching between photon-photon correlations and raman anti-correlations in a coherently prepared rb vapor. *Phys. Rev. A* **72**, 065801 (2005).
- Yang, X., Sheng, J., Khadka, U. & Xiao, M. Generation of correlated and anti-correlated multiple fields via atomic spin coherence. *Phys. Rev. A* **85**, 013824 (2012).
- McCormick, C., Boyer, V., Arimondo, E. & Lett, P. D. Strong relative intensity squeezing by four-wave mixing in rubidium vapor. *Opt. Lett.* **32**, 178–180 (2007).
- Pooser, R., Marino, A., Boyer, V., Jones K. & Lett, P. D. Quantum correlated light beams from non-degenerate four-wave mixing in an atomic vapor: The d1 and d2 lines of 85 rb and 87 rb. *Opt. Express*, **17**, 16722–16730 (2009).
- Bencheikh, K., Huntziger, E. & Levenson, J. A. Quantum noise reduction in quasi-phase-matched optical parametric amplification. *Opt. Soc. Am. B*, 12847 (1995).
- Levenson, J. A., Abram, I. & Rivera, Th. Reduction of quantum noise in optical parametric amplification. *Opt. Soc. Am. B*, 2233 (1993).
- Chen, H., Qin, M., Zhang, Y., Zhang, X., Wen, F., Wen, J. & Zhang, Y. Parametric amplification of dressed multi-wave mixing in atomic ensemble. *Laser Phys. Lett.* **11**(4), 045201 (2014).

## Acknowledgements

This work was supported by the 973 Program (2012CB921804), NSFC (11474228, 61308015, 61205112), KSTIT of Shaanxi Province (2014KCT-10).

## Author Contributions

I.A. wrote the main manuscript and contributed to experimental analysis. R.W. and Y.Z. provided the idea. Z.Z., F.W., D.Z. and C.L. contributed to the presentation and execution of the theoretical work. All authors discussed the results and contributed to the writing of the manuscript.

## Additional Information

**Competing financial interests:** The authors declare no competing financial interests.

**How to cite this article:** Ahmed, I. *et al.* Switching Correlation and Noise Level in  $\text{Pr}^{3+}:\text{YSO}$  Crystal via Dressing Nonlinear Phase. *Sci. Rep.* **6**, 33568; doi: 10.1038/srep33568 (2016).



This work is licensed under a Creative Commons Attribution 4.0 International License. The images or other third party material in this article are included in the article's Creative Commons license, unless indicated otherwise in the credit line; if the material is not included under the Creative Commons license, users will need to obtain permission from the license holder to reproduce the material. To view a copy of this license, visit <http://creativecommons.org/licenses/by/4.0/>

© The Author(s) 2016